ADVANCED FUNCTIONAL MATERIALS
www.afm-journal.de

All-Dielectric Programmable Huygens' Metasurfaces

Aleksandrs Leitis, Andreas Heßler, Sophia Wahl, Matthias Wuttig, Thomas Taubner, Andreas Tittl, and Hatice Altug**

Low-loss nanostructured dielectric metasurfaces have emerged as a breakthrough platform for ultrathin optics and cutting-edge photonic applications, including beam shaping, focusing, and holography. However, the static nature of their constituent materials has traditionally limited them to fixed functionalities. Tunable all-dielectric infrared Huygens' metasurfaces consisting of multi-layer Ge disk meta-units with strategically incorporated non-volatile phase change material $Ge_3Sb_2Te_6$ are introduced. Switching the phase-change material between its amorphous and crystalline structural state enables nearly full dynamic light phase control with high transmittance in the mid-IR spectrum. The metasurface is realized experimentally, showing post-fabrication tuning of the light phase within a range of 81% of the full 2π phase shift. Additionally, the versatility of the tunable Huygen's metasurfaces is demonstrated by optically programming the spatial light phase distribution of the metasurface with single meta-unit precision and retrieving high-resolution phase-encoded images using hyperspectral measurements. The programmable metasurface concept overcomes the static limitations of previous dielectric metasurfaces, paving the way for "universal" metasurfaces and highly efficient, ultracompact active optical elements like tunable lenses, dynamic holograms, and spatial light modulators.

1. Introduction

Metasurfaces have emerged as one of the most exciting research directions in optics, where light scattering properties of materials can be controlled at will by designing subwavelength structures ("meta-units") that strongly interact with the incident light.[1–8] While originally only enabling static functionality,[9] these concepts have recently been extended towards active optical devices by employing tunable metasurfaces for sensing and light focusing applications, where the optical response can be controlled using light inclination,[10–12] stretchable substrates,[13] electrostatic biasing of two-dimensional (2D) materials such as graphene,[14,15] and phase change materials.[16–18]

Phase change materials such as germanium antimony telluride compounds ($(GeTe)_x$-(Sb_2Te_3)), short GST, are especially promising for tunable applications[19] because their non-volatile phases (amorphous and crystalline) at room temperature enable high optical contrast with fast switching speeds.[20] This pronounced contrast between the phases originates from a unique bonding mechanism, referred to as "meta-valent bonding."[21–23] In particular, GST layers can be switched from the amorphous to the crystalline state by increased temperature or optical or electrical pulses.[24] They can be re-amorphised using a melt-quench process, where the crystalline GST is heated over the melting point and then rapidly cooled down on nanosecond time scales.[19] Intermediate crystallization states of phase transition can also be accessed, enabling continuous tuning of the material properties.[25]

So far, most tunable metasurface approaches were realized by placing plasmonic resonators on top of thin phase change material films with thicknesses of 10 to 100 nm. Several plasmonics-based reconfigurable metasurface applications have already been demonstrated, including beam steerers,[26] bifocal cylindrical lenses,[27] tunable antennas,[28] perfect absorbers,[29] and circular dichroism.[30] Even more complex electromagnetic wave phase coding has been demonstrated in the GHz spectral range with metal-based antennas.[31–34] However, the high ohmic losses of metals and tunable materials like graphene and VO_2 constrain plasmonic metasurfaces in the infrared spectral range to low transmission efficiencies,[35,36] limiting the realization of practical optical elements such as lenses and phase plates.

To overcome the losses associated with plasmonic geometries, new types of metasurfaces based on all-dielectric particles have emerged, where the strong optical response is provided

A. Leitis, Dr. A. Tittl,[+] Prof. H. Altug
Institute of Bioengineering
École Polytechnique Fédérale de Lausanne (EPFL)
Lausanne 1015, Switzerland
E-mail: andreas.tittl@epfl.ch; hatice.altug@epfl.ch
A. Heßler, S. Wahl, Prof. M. Wuttig, Prof. T. Taubner
Institute of Physics (IA)
RWTH Aachen University
Aachen 52056, Germany
The ORCID identification number(s) for the author(s) of this article can be found under https://doi.org/10.1002/adfm.201910259.
[+]Present address: Chair in Hybrid Nanosystems, Nanoinstitute Munich, Faculty of Physics, Ludwig-Maximilians-Universität München, 80539, Munich, Germany

DOI: 10.1002/adfm.201910259

by displacement currents rather than ohmic currents,[37] therefore significantly reducing the intrinsic losses of the resonators. Furthermore, the oscillating displacement current loops in dielectric resonators can provide a stronger magnetic response compared to the plasmonics,[38] allowing to combine both electric and magnetic modes to create so-called Huygens' metasurfaces with unprecedented near-unity transmission and full optical phase control.[39] This in turn enables imparting arbitrary phase patterns onto these metasurfaces, leading to the generation of freely designable holograms.[6]

Even though tunable resonators composed solely out of GST have been proposed,[40–42] their large sizes make such bulk GST structures challenging to switch between amorphous and crystalline phases. In an alternative approach, localized high refractive index regions can be embedded within a thin GST film using laser writing, enabling the realization of functionalities like greyscale holograms, reconfigurable Fresnel zone plates, and super-oscillatory lenses at visible and near-infrared wavelength ranges.[43,44] In combination with polar crystal substrates, this was also employed to produce erasable ultra-confined surface phonon polariton resonators in the infrared wavelength range.[43] However, the low layer thicknesses required for efficient GST switching prevents such geometries from simultaneously sustaining magnetic and electric dipole modes, therefore these approaches suffer from low optical phase tunability and transmission efficiency when compared to Huygens' metasurfaces.[45]

Because of all these constraints, tunable and highly transmissive metasurfaces with complete control over the phase of light for practical optical applications are still missing. Here, we present an all-dielectric optically programmable Huygens' metasurface with high transmission efficiency and nearly complete 2π light phase control for wavefront manipulation applications. We first describe the design principle of the multi-layer and multi-material dielectric meta-units via the overlap of the magnetic and electric dipole resonances. Next, we experimentally show how these two fundamental resonances can be tuned optically by switching individual meta-units with a pulsed laser, featuring an average transmission of more than 50% and an optical phase tuning range approaching 2π. Finally, we demonstrate the versatility of our method by optically programming the spatial light phase distribution of the metasurface with single meta-unit precision and retrieving high-resolution phase-encoded images using hyperspectral measurements.

2. Metasurface Working Principle

Our programmable metasurface design consists of meta-units formed by a multi-layer dielectric disk resonator incorporating two layers of the phase-change material $Ge_3Sb_2Te_6$ (GST) around a germanium (Ge) core, which is chosen for its near zero absorption losses and high refractive index in the mid-IR spectral range (**Figure 1**a). GST exhibits strong refractive index contrast when switched between the amorphous and crystalline phases[28] as well as low absorption losses in the mid-IR range (Figure S1, Supporting Information), making it well-suited for the realization of high efficiency optical elements and devices.[28] Due to the non-volatile nature of the GST phases, intermediate crystallization states can be accessed and maintained, allowing for fine tuning of the meta-unit's optical properties.[41] The meta-unit shape and height are specifically designed to sustain

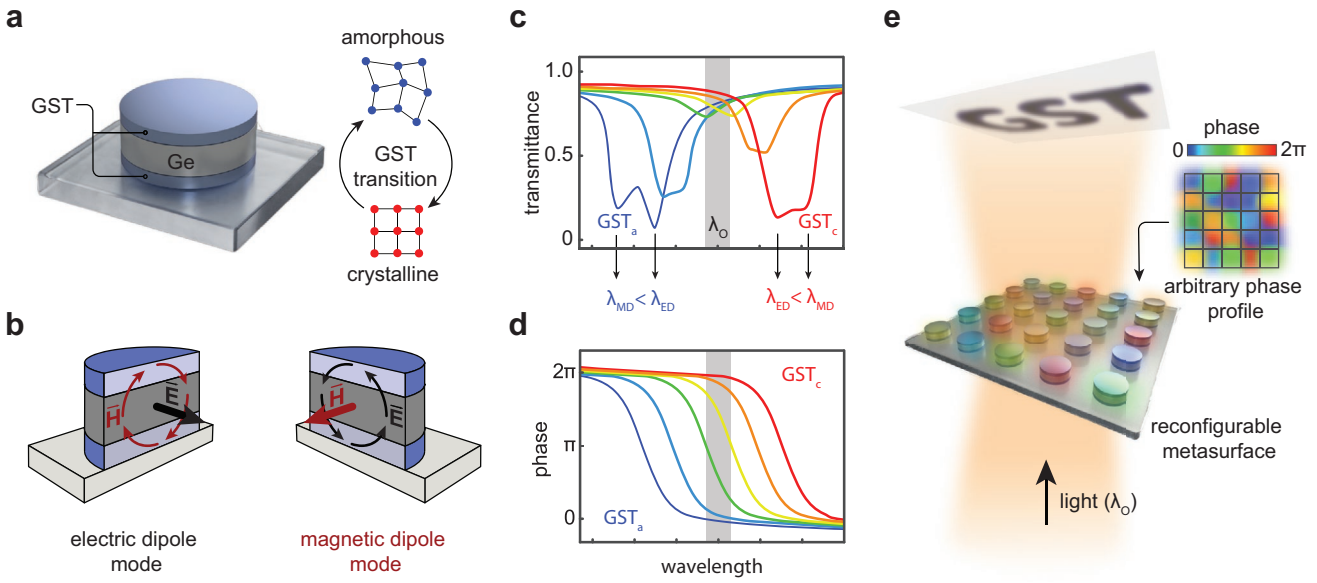

Figure 1. All-dielectric programmable Huygens' metasurfaces. a) A multi-layer dielectric meta-unit design incorporating the switchable phase-change material GST in a sandwich-like structure enables mid-IR optical phase modulation. b) The disk-shaped meta-units sustain magnetic (MD) and electric dipole (ED) resonances, where the spectral positions can be dynamically reconfigured by changing the crystallinity of the GST layers. c) The sketched optical response of the metasurface shows high transmittance at the ED and MD overlap position, where the Kerker condition is fulfilled. d) Due to contributions from both the ED and MD resonances, the sketched optical phase profile exhibits a nearly 2π phase shift across the resonance overlap position, providing full control over the propagation phase of transmitted light. e) Using ultrashort laser pulses, arbitrary spatial phase profiles can be encoded on the metasurface, enabling the realization of a multitude of programmable optical elements.

both electric dipole (ED) and magnetic dipole (MD) resonances in close spectral proximity (Figure 1b). The electric dipole mode is induced by the incident electric field, which creates a collective polarization of the dielectric meta-unit at the resonance frequency.[46] The magnetic dipole mode is characterized by an oscillating displacement current loop, which creates an associated strong magnetic dipole.

Due to the strategic GST layer placement on the top and bottom side of the meta-unit, the magnetic mode (high fields at the sides) is influenced more by the refractive index change of the GST upon crystallization than the electric mode (high fields at the center), resulting in a comparatively larger spectral shift $\Delta\lambda_{MD}$ (Figure 1c). During the crystallization, the Kerker condition[47] is satisfied, where the spectral and spatial overlap of both resonances provides constructive interference in the transmission direction and results in near perfect transmittance at the operating wavelength (λ_0, Figure 1c). The combination of the respective optical phase shifts of π associated with each resonance enables nearly full 2π phase modulation across the spectral position of resonance overlap (Figure 1d). In addition, intermediate crystallization states enable the encoding of different values of the light phase in the whole accessible phase range while maintaining high average transmittance at the operating wavelength (grey region in Figure 1c,d). Crucially, by optically switching individual meta-units of the metasurface, it is possible to write an arbitrary optical phase profile onto the surface, which enables the realization of versatile optical devices like tunable lenses, and spatial light modulators[48] (Figure 1e).

3. Meta-Unit Design and Numerical Simulations

The optimized tunable meta-unit consists of a disk with a radius of 640 nm and a unit cell periodicity of 2000 nm (**Figure 2**a). Its core is made of germanium (thickness $H_{Ge} = 330$ nm), which is surrounded by top and bottom layers of GST ($H_{GST} = 90$ nm) in a multi-layer configuration. To protect the GST from oxidation and prevent inter-atomic diffusion between the GST and Ge, additional $ZnS:SiO_2$ buffer layers of 10 nm thickness are introduced at the layer interfaces. CaF_2 is chosen as substrate material because of its low refractive index and near-zero absorption in the near- and mid-IR spectral regions.

Numerical simulations show that at the resonance frequency of the ED mode, the displacement field D is confined in the central part of the meta-unit (Figure 2b). In contrast, the displacement field for the MD resonance is also located in the bottom and the top GST layers of the meta-unit, resulting in a higher sensitivity to the GST refractive index changes during the phase transition (Figure 2c).

The numerical simulations of the metasurface's optical response were performed for different intermediate GST layer crystallization states, where a linear interpolation of the GST complex permittivity between the amorphous and crystalline states was assumed (see Supporting Information for details). The layer thickness and the disk radius are tailored to produce ED and MD modes in close spectral proximity when the GST is amorphous, with the MD mode at a slightly lower wavelength to ensure spectral overlap when the GST layer crystallizes. The spectral locations of the ED and MD modes were analyzed by probing the electric and magnetic fields at the center of the disk resonator (see Figure S2, Supporting Information).

As can be seen from the plot of transmittance over crystallization state and wavelength in Figure 2d, there is a strong spectral overlap of the ED (white curve) and MD (bright red curve) modes at a wavelength of around 3.75 μm (dashed black line), which results in high transmittance values in this spectral region. Since the bright red curve has a steeper slope than the white curve, the simulated data confirms that the MD mode is more sensitive to the changes in the GST crystallization state than the ED mode and therefore experiences larger spectral shifts. The extracted light phase spectrum from each crystallization state shows that a phase shift of nearly 2π is accessible in the operating wavelength range (Figure 2e). Finally, we specifically compare the transmittance and light phase values at the operating wavelength of 3.75 μm for each crystallization state (Figure 2f). We calculate a total light phase shift of $\Delta\varphi = 0.86 \cdot 2\pi$ with an average transmittance of 0.62. This large optical phase modulation can be used for the implementation of optical devices such as beam deflectors using programmable Huygens' metasurfaces as presented in Figure S3, Supporting Information. Furthermore, we show that our all-dielectric disk geometry confines the electric near-fields mostly inside its volume at the electric and magnetic dipole resonances, mitigating the coupling between neighboring meta-units and enabling full control of the phase profile in a straightforward manner (see Figure S3, Supporting Information). The transmission efficiency can be further improved to surpass 70% by embedding the resonators in a medium with a refractive index that matches the substrate material (see Figure S4, Supporting Information).

4. Experimental Realization

To tailor and study the mode overlap, multiple programmable metasurfaces consisting of unswitched meta-units (amorphous GST phase) with varying disk radius from 500 to 790 nm and a constant periodicity of 2000 nm were fabricated (see Section 7) and the transmittance of each array was characterized using a Fourier-transform IR (FTIR) spectrometer in combination with an infrared microscope equipped with custom-made apertures that reduce the polar and azimuthal angular spread (see Figure S5, Supporting Information).

The plot of measured transmittance over disk radius and wavelength reveals that the spectral positions of the two main modes of the system are strongly modified by the radius of the disks (**Figure 3**a). Specifically, we find an increased sensitivity of the ED mode (dashed white line) to the disk radius compared to the MD mode (dashed bright red line), therefore allowing for the fine adjustment of the individual mode positions. Figure 3b displays a scanning electron microscopy (SEM) image of part of the metasurface with $R = 630$ nm. Additionally, we performed atomic force microscopy (AFM) measurements of the height and side wall profile of a meta-unit with $R = 650$ nm, which agrees well with the expected structure height of $H = 500$ nm (Figure 3c). The corresponding numerically simulated transmittance spectra of the metasurface are in very good agreement with the FTIR measurements (Figure 3d), assuming a slightly thinner GST layer thickness of 70 nm, Ge central core thickness

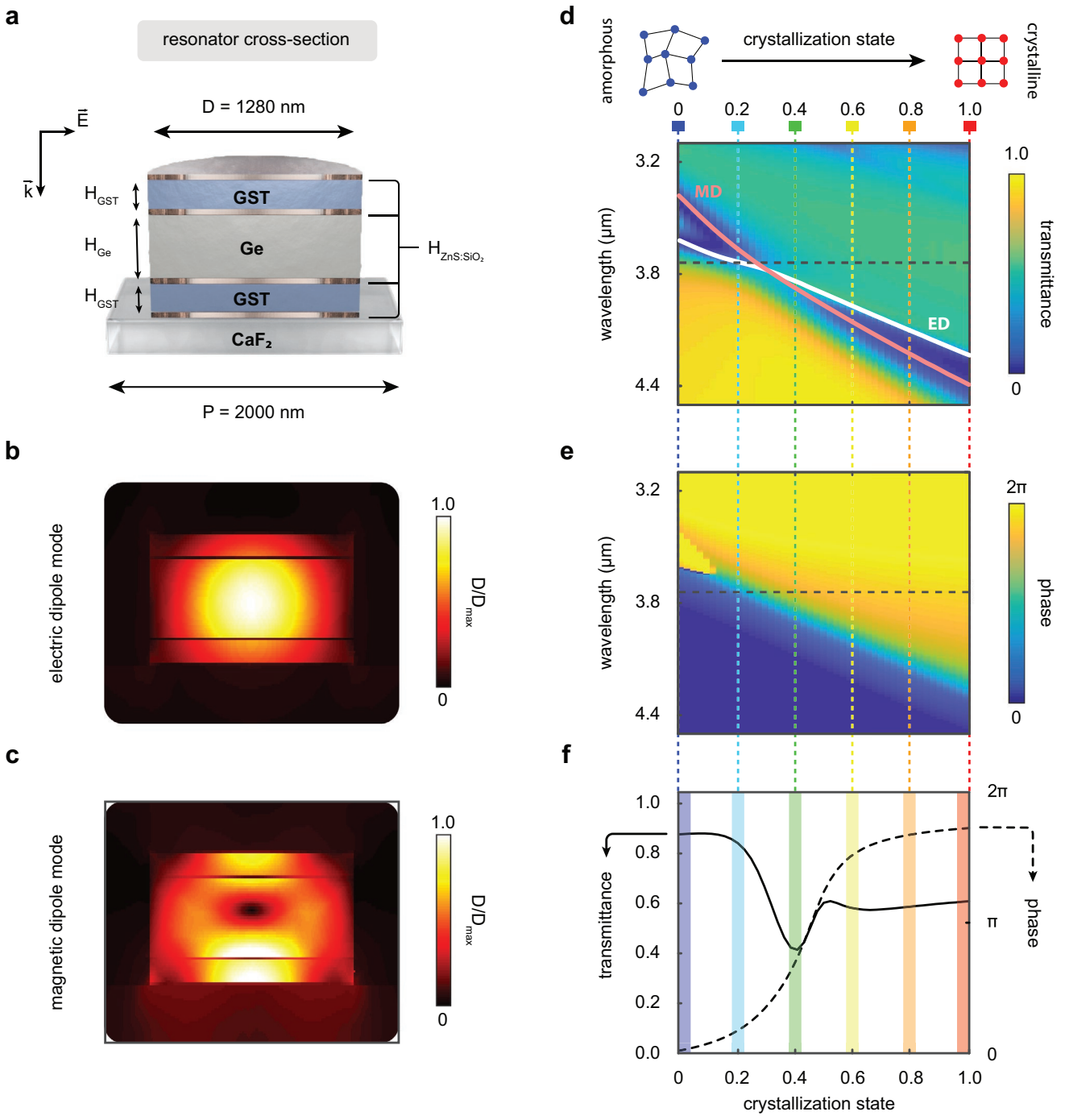

Figure 2. Huygens' meta-unit design simulations. a) Sketch of the multi-layer tunable meta-unit design, showing the CaF_2 substrate, Ge and GST resonator materials, and the $ZnS:SiO_2$ buffer layers. b,c) Simulated displacement field profile at the ED and MD resonance wavelengths, showing that the MD resonance confines the displacement field strongly in the GST layers, therefore making it more sensitive to the refractive index changes associated with the GST phase transition. d) Simulated transmittance (color-coded) of the Huygens' metasurface when the GST layers are gradually tuned from the amorphous to the crystalline state. e) Simulated transmission optical phase profiles (color-coded) for the same GST crystallization states from panel (d). f) Transmittance (solid) and light phase (dashed) values at the operating wavelength of 3.75 μm (dashed black line in (d),(e)) for all intermediate GST crystallization states.

of 325 nm and side wall tapering angle of 10°. Here, the slightly lower layer thickness could arise from deposition rate uncertainties in the sputtering process. Exemplary spectra for three different radii from both the experimental measurements and numerical simulations are displayed in Figure 3e,f, highlighting the good agreement. Interestingly, both the experimental and numerical data reveal the presence of an additional dipole mode at higher wavelengths (>4 μm), which results from the

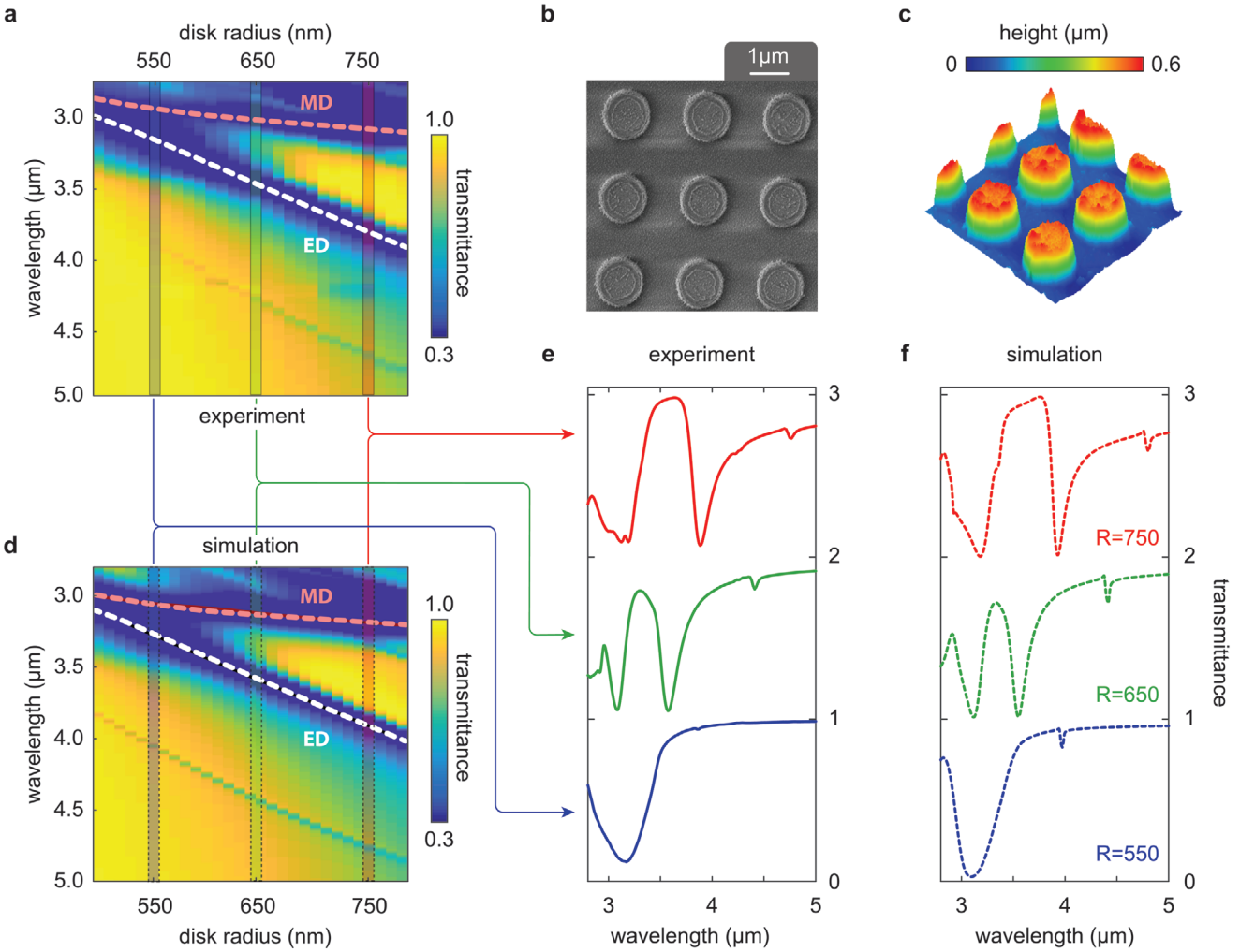

Figure 3. Geometrical tuning of mode overlap. a) Experimentally measured metasurface transmittance for meta-unit arrays with different disk radius, where the dashed lines indicate the spectral location of the ED and MD resonant modes. b) SEM micrograph of nanostructured meta-units with $R = 630$ nm. c) AFM scan of meta-units with $R = 650$ nm confirms the expected disk height. d) Numerically simulated transmittance spectra plot for different disk radii. e,f) Comparison of individual spectra for the experiments and simulations from panels (a) and (d), offset in *y*-direction for clarity with *R* values given in nanometer units.

non-normal light incidence and is associated with a displacement current loop parallel to the layer stack and a magnetic dipole pointing along the layer stack normal.

5. Metasurface Programming

Spatially selective GST crystallization was performed by means of optical switching with a pulsed laser ($\lambda_{laser} = 660$ nm $\ll \lambda_0$), enabling precise control of the location and crystallization state, where increasing laser pulse powers were leveraged to obtain higher levels of GST layer crystallization (**Figure 4**a). Thus, individual meta-units can be switched to different crystallization states, enabling true optical programming of the metasurface.[28] Accordingly, individual subarrays of the disk array with $R = 650$ nm were optically switched and then characterized with a 2D focal plane array imaging detector attached to the FTIR spectrometer (Bruker Vertex 70), allowing to measure the spectral response of multiple neighboring subarrays and different material states simultaneously with micrometer pixel resolution. Each disk antenna was switched individually with a single laser pulse of 500 ns duration and varying pulse power (see Section 7 for details). The spectra extracted from hyperspectral imaging data show that the resonance position exhibits a pronounced spectral shift with increased laser pulse power (Figure 4b). The numerical simulations with intermediate crystallization states are in good agreement with the measured data and confirm the ED and MD mode overlap at a wavelength of around 3.75 μm. The sidewall tapering and inclined light incident angle perturb the ED and MD modes, reducing the metasurface transmission efficiency at the ED and MD resonance overlap. Nevertheless, the average transmittance for all crystallization states at the operation wavelength $\lambda_0 = 3.75$ μm still remains over 53%, while the extracted light phase from the numerical data demonstrates a modulation of 81% of the full 2π phase shift (see Figure 4c and Figure S6,

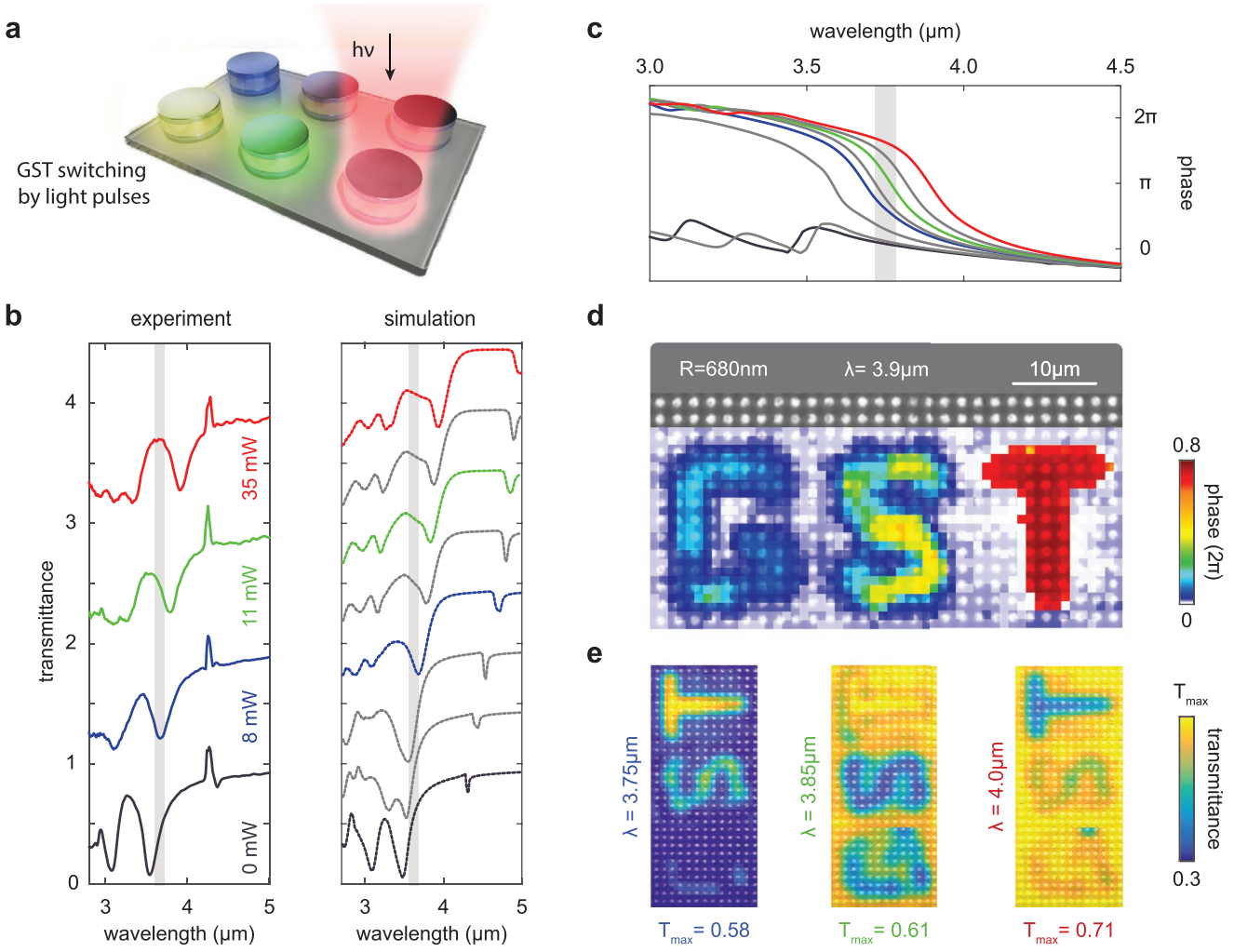

Figure 4. All-optical metasurface programming. a) The crystallization states of individual meta-units are controlled by illumination with ultrashort laser pulses with a pulsed laser (λ_{laser} = 660 nm ≪ λ_0), enabling spatial control over the transmission phase profile. b) Experimental and simulated metasurface transmission for different crystallization states of the GST (prepared experimentally with the denoted laser powers), where grey curves show additional simulated intermediate crystallization states. A clear shift of the resonance across the operation wavelength λ_0 = 3.75 μm is observed (grey shaded area). The features at 4.3 μm originate from ambient CO_2 absorption. c) Simulations of the light phase spectra for the crystallization states in (b). Extracted phase values at λ_0 = 3.75 μm (grey line) confirm nearly complete 2π phase control. d) Programming of arbitrary spatial light phase distributions is demonstrated by encoding the letters "G," "S," and "T" into our metasurface with different crystallization states, that is, light phase (color-coded). The image is overlaid over an optical micrograph of the metasurface. e) Color-coded transmittance images for different resonance positions, highlighting the spatial light modulation capabilities of our programmable metasurface, where T_{max} denotes the maximum transmittance value at the specific wavelength.

Supporting Information). Moreover, the transmittance minimum in Figure 4b shifts by around $\Delta\lambda$ = 360 nm, resulting in a tuning figure of merit of TFOM = $\Delta\lambda$/FWHM = 1.8, where the full-width-half-maximum (FWHM) of the amorphous state was taken as the reference. Thus, the transmittance can be tuned from in-resonance to completely out-of-resonance, enabling transmittance modulations of up to 60%. Additionally, we show reversible switching of the GST multi-layer system by a re-amorphization and re-crystallization process (Figure S7, Supporting Information).

In order to demonstrate the optical programming of our Huygens' metasurface, we encoded images of the letters "G," "S," and "T" into the metasurface with R = 680 nm by switching the individual meta-units to different crystallization states (Figure S8, Supporting Information). The change in the resonant properties is confirmed with data from the hyperspectral imaging measurements, which allow to directly correlate the spectral information with the simulated light phase. The metasurface induced light phase shift is displayed pixel by pixel in a color-coded spatial light phase map (Figure 4d). The spectrally imaged light phase is overlaid on top of an optical micrograph of the metasurface, confirming the accurate addressing of single meta-units by our laser switching method. We further demonstrate that not only the optical phase can be tuned, but also the transmission of the metasurface can be controlled in the spectral range around the operation wavelength in Figure 4e, where the transmittance data is displayed over the optical micrograph of the metasurface. The

hyperspectral imaging data shows that the transmission can be gradually tuned and high contrast can be obtained at different spectral locations. Therefore, our multi-layered dielectric meta-unit design provides nearly complete control of light phase and transmission, which can be arbitrary programmed with single meta-unit precision, making this method ideally suited for diverse applications like tunable lenses or dynamic beam shaping. In order to demonstrate the versatility of our Huygens' metasurfaces we studied beam focusing and manipulations in Figure S9, Supporting Information.

6. Conclusions

We have demonstrated a novel metasurface-based concept for nearly full light phase control with high transmission efficiency. Specifically, we incorporated the phase change material $Ge_3Sb_2Te_6$ in the all-dielectric multi-layer meta-unit design, which enables dynamic control of the spectral overlap between ED and MD modes. Thus, each meta-unit acts as a Huygens' source with variable light phase. The numerical simulations show near 2π phase shift upon GST layer crystallization with average transmittance above 50%. We experimentally realized such a metasurface by nanofabrication and characterized its performance with FTIR spectral measurements, which showed very good agreement with the numerical simulations. In order to demonstrate the versatility of our method, we optically programmed a light phase profile into the metasurface with single meta-unit precision and a maximum light phase tunability of 81% of full 2π. The encoded images were extracted with hyperspectral measurements. Our method targets the important mid-IR spectral window where it could enable applications in key areas like adaptive optics in astronomy, infrared imaging for defence and security, free-space optical communication, and remote sensing. Moreover, with emerging low-loss phase change materials at near-infrared and visible frequencies, the operational spectral window of the active metasurfaces can be further expanded.[49,50] Therefore, our method provides an attractive platform for programmable and efficient wave front manipulation for a wide range of applications from tunable lenses and beam shapers to dynamic holograms and active image correction.

7. Experimental Section

Numerical Simulations: The metasurface optical performance was simulated using the finite-difference time-domain software CST microwave studio. The CaF_2 substrate was assumed to be lossless and with non-dispersive refractive index $n_{sub} = 1.4$. The $ZnS:SiO_2$ buffer layers were assumed to be lossless with a refractive index $n_{buffer} = 1.6$, while the germanium was assumed to be lossless with an average refractive index of $n_{Ge} = 4.03$. The GST was simulated with the real part of the complex permittivity as displayed in the Figure S1, Supporting Information. For the Figures 3 and 4, the numerical simulations were performed assuming light inclination angle of 18° with angular spread from 16° to 20° and s-polarization state. For the numerical simulations in Figure 4b, uniform crystallization on both top and bottom GST layers were assumed, which gives good agreement with the experimental data. However, for more accurate description of the crystallization profile during optical switching, multiphysics simulations should be taken into account.[48]

Metasurface Fabrication: The GST and Ge layers were sputtered with direct current magnetron sputtering while $ZnS:SiO_2$ buffer layers were deposited by radio frequency magnetron sputtering. The GST was in the amorphous phase after deposition. The resonator pattern was written by electron beam lithography in double layer poly methyl methacrylate (PMMA) photoresist with different molecular weights (500 nm 495 K PMMA and 70 nm 950 K PMMA). A hard mask of 100 nm Al_2O_3 was deposited by electron beam evaporation. Subsequently, a lift-off process was performed to obtain the hard mask pattern. The disk patterns were transferred into the underlying layer stack by ICP plasma etching with Ar/CF_4 gas mixture ratio 50/10 sccm, RF power of 300 W, and chamber pressure of 50 mTorr. In order not to damage the GST layers and as the hard mask only slightly perturbs the overall performance, the remaining hard mask was not removed.

Optical Measurements: The optical response of the multi-layer meta-units was characterized under ambient conditions with a FTIR spectrometer (Bruker Vertex 70) equipped with an infrared microscope (Hyperion 3000) and operated in transmission mode. The microscope's reflective Cassegrain objective has a numerical aperture (NA) of 0.4 with 15× magnification and a central inclination angle of 18° with an angular spread from 10° to 24°. The IR microscope was also equipped with a focal plane array with hyperspectral imaging capability. The objective was equipped with custom-made apertures that reduce the polar and azimuthal angular spread, as shown in Figure S5, Supporting Information. For normalization, hyperspectral images of the CaF_2 substrate were taken. The FTIR spectra presented in Figure 4 result from averaging over all pixels in a $20 \times 20\ \mu m^2$ meta-unit subarray region.

Optical Switching Experiments: Optical switching of the phase change material GST was realized by a custom-made laser setup.[43,48] The light from a red, pulsed laser diode (λ = 660 nm) was focused through a 10× objective with a numerical aperture of 0.5 onto the sample surface. The sample was placed on a Thorlabs NanoMax-TS (Max311/M) stage, which is movable in *x*, *y*, and *z* direction and connected to a Thorlabs closed-loop piezo controller (BPC303). A custom program allowed for the automated positioning of pulsed laser shots on the sample surface within 5 nm accuracy. In order to switch the GST to different crystallization states, the pulse duration of the laser diode was kept constant at 500 ns while the pulse power was varied between 0 and 35 mW. Each targeted meta-unit was switched by a single light pulse.

Supporting Information

Supporting Information is available from the Wiley Online Library or from the author.

Acknowledgements

The research leading to these results has received funding from the European Research Council (ERC) under grant agreement no. 682167 VIBRANT-BIO and the European Union Horizon 2020 Framework Programme for Research and Innovation under grant agreements no. 665667 (call 2015), no. 777714 (NOCTURNO project). This work was also supported by the German Federal Ministry of Education and Research within the funding program Photonics Research Germany (contract number 13N14151) and the DFG (German Science Foundation) within the collaborative research center SFB 917 "Nanoswitches." The authors also acknowledge École Polytechnique Fédérale de Lausanne and Center of MicroNano Technology for nanofabrication, and J. Gao for the sputter deposition of the thin film layer stacks.

Conflict of Interest

The authors declare no conflict of interest.

Author Contributions

A.L. and A.H. contributed equally to this work. A.L., A.T., T.T., and H.A. conceived and designed the research; A.L. and A.H. fabricated the dielectric metasurfaces; A.L., S.W., and A.H. carried out optical measurements and analyzed data; A.H. and S.W. performed the optical switching experiments; A.L. carried out numerical simulations; M.W. provided the necessary equipment for material deposition; and all authors contributed to writing the manuscript.

Keywords

adaptive optics, dielectric metasurfaces, phase-change materials, programmable metasurfaces, wavefront control

Received: December 9, 2019
Revised: January 21, 2020
Published online: March 12, 2020

[1] A. Arbabi, Y. Horie, M. Bagheri, A. Faraon, *Nat. Nanotechnol.* **2015**, *10*, 937.
[2] N. Yu, P. Genevet, M. A. Kats, F. Aieta, J.-P. Tetienne, F. Capasso, Z. Gaburro, *Science* **2011**, *334*, 333.
[3] F. Qin, L. Ding, L. Zhang, F. Monticone, C. C. Chum, J. Deng, S. Mei, Y. Li, J. Teng, M. Hong, S. Zhang, A. Alù, C. W. Qiu, *Sci. Adv.* **2016**, *2*, e1501168.
[4] S. Wang, P. C. Wu, V. C. Su, Y. C. Lai, M. K. Chen, H. Y. Kuo, B. H. Chen, Y. H. Chen, T. T. Huang, J. H. Wang, R. M. Lin, C. H. Kuan, T. Li, Z. Wang, S. Zhu, D. P. Tsai, *Nat. Nanotechnol.* **2018**, *13*, 227.
[5] R. C. Devlin, M. Khorasaninejad, W. T. Chen, J. Oh, F. Capasso, *Proc. Natl. Acad. Sci. USA* **2016**, *113*, 10473.
[6] F. Ding, A. Pors, S. I. Bozhevolnyi, *Rep. Prog. Phys.* **2018**, *81*, 026401.
[7] A. Tittl, A. Leitis, M. Liu, F. Yesilkoy, D.-Y. Choi, D. N. Neshev, Y. S. Kivshar, H. Altug, *Science* **2018**, *360*, 1105.
[8] A. Tittl, A. John-Herpin, A. Leitis, E. R. Arvelo, H. Altug, *Angew. Chem., Int. Ed.* **2019**, *58*, 14810.
[9] H.-T. Chen, A. J. Taylor, N. Yu, *Rep. Prog. Phys.* **2016**, *79*, 076401.
[10] S. M. Kamali, E. Arbabi, A. Arbabi, Y. Horie, M. S. Faraji-Dana, A. Faraon, *Phys. Rev. X* **2017**, *7*, 041056.
[11] T. W. W. Maß, T. Taubner, *ACS Photonics* **2015**, *2*, 1498.
[12] A. Leitis, A. Tittl, M. Liu, B. H. Lee, M. B. Gu, Y. S. Kivshar, H. Altug, *Sci. Adv.* **2019**, *5*, eaaw2871.
[13] E. Arbabi, A. Arbabi, S. M. Kamali, Y. Horie, M. S. Faraji-Dana, A. Faraon, *Nat. Commun.* **2018**, *9*, 812.
[14] D. Rodrigo, O. Limaj, D. Janner, D. Etezadi, F. J. G. de Abajo, V. Pruneri, H. Altug, *Science* **2015**, *349*, 165.
[15] S. Kim, M. S. Jang, V. W. Brar, K. W. Mauser, L. Kim, H. A. Atwater, *Nano Lett.* **2018**, *18*, 971.
[16] Z. L. Samson, K. F. MacDonald, F. De Angelis, K. Knight, C. C. Huang, E. Di Fabrizio, D. W. Hewak, N. I. Zheludev, *Appl. Phys. Lett.* **2010**, *96*, 143105.
[17] T. Paik, S. H. Hong, E. A. Gaulding, H. Caglayan, T. R. Gordon, N. Engheta, C. R. Kagan, C. B. Murray, *ACS Nano* **2014**, *8*, 797.
[18] C. U. Hail, A. U. Michel, D. Poulikakos, H. Eghlidi, *Adv. Opt. Mater.* **2019**, *7*, 1801786.
[19] M. Wuttig, H. Bhaskaran, T. Taubner, *Nat. Photonics* **2017**, *11*, 465.
[20] D. Loke, T. H. Lee, W. J. Wang, L. P. Shi, R. Zhao, Y. C. Yeo, T. C. Chong, S. R. Elliott, *Science* **2012**, *336*, 1566.
[21] M. Zhu, O. Cojocaru-Mirédin, A. M. Mio, J. Keutgen, M. Küpers, Y. Yu, J. Y. Cho, R. Dronskowski, M. Wuttig, *Adv. Mater.* **2018**, *30*, 1706735.
[22] M. Wuttig, V. L. Deringer, X. Gonze, C. Bichara, J. Y. Raty, *Adv. Mater.* **2018**, *30*, 1803777.
[23] J. Y. Raty, M. Schumacher, P. Golub, V. L. Deringer, C. Gatti, M. Wuttig, *Adv. Mater.* **2019**, *31*, 1806280.
[24] F. Ding, Y. Yang, S. I. Bozhevolnyi, *Adv. Opt. Mater.* **2019**, *7*, 1801709.
[25] Y. G. Chen, T. S. Kao, B. Ng, X. Li, X. G. Luo, B. Luk'yanchuk, S. A. Maier, M. H. Hong, *Opt. Express* **2013**, *21*, 13691.
[26] C. R. de Galarreta, A. M. Alexeev, Y. Y. Au, M. Lopez-Garcia, M. Klemm, M. Cryan, J. Bertolotti, C. D. Wright, *Adv. Funct. Mater.* **2018**, *28*, 1704993.
[27] X. Yin, T. Steinle, L. Huang, T. Taubner, M. Wuttig, T. Zentgraf, H. Giessen, *Light: Sci. Appl.* **2017**, *6*, e17016.
[28] A. K. U. Michel, D. N. Chigrin, T. W. W. Maß, K. Schönauer, M. Salinga, M. Wuttig, T. Taubner, *Nano Lett.* **2013**, *13*, 3470.
[29] A. Tittl, A. K. U. Michel, M. Schäferling, X. Yin, B. Gholipour, L. Cui, M. Wuttig, T. Taubner, F. Neubrech, H. Giessen, *Adv. Mater.* **2015**, *27*, 4597.
[30] X. Yin, M. Schäferling, A. K. U. Michel, A. Tittl, M. Wuttig, T. Taubner, H. Giessen, *Nano Lett.* **2015**, *15*, 4255.
[31] T. J. Cui, M. Q. Qi, X. Wan, J. Zhao, Q. Cheng. *Light: Sci. Appl.* **2014**, *3*, e218.
[32] X. G. Zhang, W. X. Tang, W. X. Jiang, G. D. Bai, J. Tang, L. Bai, C. W. Qiu, T. J. Cui, *Adv. Sci.* **2018**, *5*, 1801028.
[33] X. Ding, F. Monticone, K. Zhang, L. Zhang, D. Gao, S. N. Burokur, A. de Lustrac, Q. Wu, C. W. Qiu, A. Alù, *Adv. Mater.* **2015**, *27*, 1195.
[34] K. Chen, Y. Feng, F. Monticone, J. Zhao, B. Zhu, T. Jiang, L. Zhang, Y. Kim, X. Ding, S. Zhang, A. Alù, C. W. Qiu, *Adv. Mater.* **2017**, *29*, 1606422.
[35] F. Monticone, N. M. Estakhri, A. Alù, *Phys. Rev. Lett.* **2013**, *110*, 203903.
[36] H. Cheng, S. Chen, P. Yu, W. Liu, Z. Li, J. Li, B. Xie, J. Tian, *Adv. Opt. Mater.* **2015**, *3*, 1744.
[37] A. I. Kuznetsov, A. E. Miroshnichenko, M. L. Brongersma, Y. S. Kivshar, B. Luk'yanchuk, *Science* **2016**, *354*, aag2472.
[38] J. A. Schuller, R. Zia, T. Taubner, M. L. Brongersma, *Phys. Rev. Lett.* **2007**, *99*, 107401.
[39] Y. H. Fu, A. I. Kuznetsov, A. E. Miroshnichenko, Y. F. Yu, B. Luk'yanchuk, *Nat. Commun.* **2013**, *4*, 1527.
[40] C. H. Chu, M. L. Tseng, J. Chen, P. C. Wu, Y.-H. Chen, H.-C. Wang, T.-Y. Chen, W. T. Hsieh, H. J. Wu, G. Sun, D. P. Tsai, *Laser Photonics Rev.* **2016**, *10*, 986.
[41] J. Tian, H. Luo, Y. Yang, F. Ding, Y. Qu, D. Zhao, M. Qiu, S. I. Bozhevolnyi, *Nat. Commun.* **2019**, *10*, 396.
[42] J. Tian, Q. Li, J. Lu, M. Qiu, *Opt. Express* **2018**, *26*, 23918.
[43] P. Li, X. Yang, T. W. W. Maß, J. Hanss, M. Lewin, A.-K. U. Michel, M. Wuttig, T. Taubner, *Nat. Mater.* **2016**, *15*, 870.
[44] Q. Wang, E. T. F. Rogers, B. Gholipour, C. M. Wang, G. Yuan, J. Teng, N. I. Zheludev, *Nat. Photonics* **2016**, *10*, 60.
[45] M. Decker, I. Staude, M. Falkner, J. Dominguez, D. N. Neshev, I. Brener, T. Pertsch, Y. S. Kivshar, *Adv. Opt. Mater.* **2015**, *3*, 813.
[46] J. van de Groep, A. Polman, *Opt. Express* **2013**, *21*, 26285.
[47] M. Kerker, D.-S. Wang, C. L. Giles, *J. Opt. Soc. Am.* **1983**, *73*, 765.
[48] A. U. Michel, A. Heßler, S. Meyer, J. Pries, Y. Yu, T. Kalix, M. Lewin, J. Hanss, A. De Rose, T. W. W. Maß, M. Wuttig, D. N. Chigrin, T. Taubner, *Adv. Mater.* **2019**, *31*, 1901033.
[49] Q. Zhang, Y. Zhang, J. Li, R. Soref, T. Gu, J. Hu, *Opt. Lett.* **2018**, *43*, 94.
[50] W. Dong, H. Liu, J. K. Behera, L. Lu, R. J. H. Ng, K. V. Sreekanth, X. Zhou, J. K. W. Yang, R. E. Simpson, *Adv. Funct. Mater.* **2019**, *29*, 1806181.